High performance microfluidic capillary electrophoresis devices

Lung-Ming Fu · Jik-Chang Leong · Chiu-Feng Lin · Chang-Hsien Tai · Chien-Hsiung Tsai

Abstract This paper presents a novel microfluidic capillary electrophoresis (CE) device featuring a double-T-form injection system and an expansion chamber located at the inlet of the separation channel. This study addresses the principal material transport mechanisms depending on parameters such as the expansion ratio, the expansion length, the fluid flow. Its design utilizes a double-L injection technique and combines the expansion chamber to minimize the sample leakage effect and to deliver a high-quality sample plug into the separation channel so that the detection performance of the device is enhanced. Experimental and numerical testing of the proposed microfluidic device that integrates an expansion chamber located at the inlet of the separation channel confirms its ability to increase the separation efficiency by improving the sample plug shape and orientation. The novel microfluidic capillary electrophoresis device presented in this paper has demonstrated a sound potential for future use in high-quality, high-throughput chemical analysis applications and throughout the micro-total-analysis systems field.

Keywords Microfluidic capillary electrophoresis device · Injection system · Expansion chamber

L.-M. Fu
Department of Materials Engineering,
National Pingtung University of Science and Technology,
Pingtung, Taiwan 912

J.-C. Leong · C.-F. Lin · C.-H. Tai · C.-H. Tsai (✉)
Department of Vehicle Engineering,
National Pingtung University of Science and Technology,
Pingtung, Taiwan 912
e-mail: chtsai@mail.npust.edu.tw

1 Introduction

Micro total analysis system (μ-TAS), also known as "microfluidic devices," can dramatically innovate the way chemical and biochemical assays are performed (Tian et al. 2005; Li et al. 2005; Wei et al. 2006; Wu and Yang 2006; Lee et al. 2006; Bown and Meinhart 2006). The beauty of this technique lies in its ability to separate a sample with increased speed, reduced sample consumption, and higher throughput (Du et al. 2005). Using microfabrication technology, a network of microchannels could be manufactured on a microchip made of glass, quartz, PMMA (polymethylmethacrylate), PDMS (poly-dimethylsiloxane), and PC (polycarbonate) substrate to form an integrated microfluidic chip capable of performing a variety of procedures, including sample loading, handling, mixing, sorting, counting, chemical reaction, pretreatment, separation, etc. (Xiang et al. 2005; Gao et al. 2005; Coleman and Sinton 2005; Erickson 2005; Nguyen and Huang 2006; Saadi et al. 2006; Wang et al. 2006; Tsai et al. 2007). In recent "lab-on-a-chip" concepts, a wide variety of functional components have been integrated serially into a microchip in order to carry out a complete assay of biomaterials, e.g. DEP-CE for cell collection and separation (Huang et al. 2003; Zou et al. 2006), PCR-CE for rapid DNA reproduction and analysis (Gong et al. 2006; Chang et al. 2006), self-actuated integrated thermo-responsive hydrogel valves for PCR system (Wang et al. 2005a,b), micro flow cytometers integrating optical fibers for the on-line detection of cells sorting and counting (Fu et al. 2004), micro flow cytometers integrating dielectrophoresis force for three-dimensilnal focusing of cells sorting (Lin et al. 2004a), and microfluidic chips combined micromagnetic for separation of living cells (Xia et al. 2006).

In a microfluidic capillary electrophoresis chip, an important component of a typical microfluidic chip is the injection and separation processes of a microfluidic device, which is a cross-type microchannel that employs electrokinetic flow to load samples into the intersection from one channel and dispense a minute quantity of sample into another channel. The precise control of the sample injection and separation processes amount in microfluidic dispensers is key to the analysis processes. Therefore, a thorough understanding of the mechanisms governing electrokinetic manipulations, particularly those associated with discrete injections and separations, is essential when seeking to optimize the design of compact microchips. A large number of researchers have investigated the sample transport phenomena in microfluidic capillary electrophoresis chips. Seiler et al. (1993) firstly integrated sample injection and separation system on a planar glass chip and used to perform micro capillary electrophoresis chip analysis. The feasibility of using electrokinetic pumping to transport samples in the manifold of microchannels was confirmed and the successful execution of electrophoresis separation on glass substrates had been demonstrated.

For electrokinetical injection types, the design of injectors for microfluidic devices was based on the floating sample introduction method, where voltages are only applied to the sample injection/sample waste channels during the injection stage, leaving the buffer/separation channels to float (Crabtree et al. 2001; Wu et al. 2004; Ren and Li 2004; Tsai et al. 2005a; Wenclawiak and Püschl 2006). The floating sample injection method induces a sample leakage effect, which reduces the separation efficiency of a device since the results in an increasing signal baseline as the number of injection runs increases (Fu and Lin 2003, 2004; Lin et al. 2004a,b,c; Tsai et al. 2005a, 2006a,b). To develop viable low-leakage injection techniques with the ability to circumvent the sample leakage problem and to improve the definition of the injected sample plug of microfluidic devices, pinched, gated, pullback, and double-L injection method introduction protocols have been proposed. Pinched voltage applied at the buffer inlet and outlet induces a buffer flow toward the sample waste reservoir to counteract the dispersion of sample into the separation channel. Ermakov et al. (2000, Alarie et al. 2001; Fu et al. 2003; Luo et al. 2006; Zhuang et al. 2006) used computer simulation to investigate the electrokinetic focusing on the cross-intersection of microchannels and the voltage parameters for the pinched and gated injection schemes. Slentz et al. (2002) considered the sampling bias induced by differences in analyte turning in gated injections. Ren et al. (2003; Sinton et al. 2003) developed a three-step technique for discrete sample injections in straight-cross microfluidic chips. The proposed technique modified the pinched valve injection method by

adding an intermediate dynamic injection step, in which the sample was pumped directly into the intersection and three connecting channels. Baldock et al. (2004) presented a variable volume injector for sample delivery in a miniaturized isotachophoretic device based on hydrodynamic pumping in the injector and electrokinetic pumping in the separator. Implementing a U-shaped injection channel angled at 45° in a syringe pump based sample handling system was found to improve the resolution of the injected zones. The double-L injection method employs an initial force to limit the leakage effect induced in the floating sample injection method. Flow direction is not as in a standard injection across the microchannel but around the corner of the microchannel cross. The low leakage injection technique was studied in great detail by the research group of Fu both experimentally and numerically (Fu and Lin 2003; Lin et al. 2004a,b,c; Tsai et al. 2005a, 2006a,b).

For separation process, since the electrophoresis separation microchannels are generally designed within a compact area in a microfabricated chip, it is necessary to utilize a serpentine channel configuration if the required separation length is to be achieved. In attempting to increase separation efficiency while simultaneously decreasing production cost and enhancing device miniaturization, recent studies have investigated a variety of different serpentine microchannel configurations. Culbertson et al. (1998) presented a study of dispersion caused by constant radius turns where the radius of curvature was at least 2.5 times greater than the width of the channel. The dispersion created by microchannel turns is caused by differences in both path length and electric field strength in the turn. The stretching of the analytical band as it traverses a turn in the curved microchannel is commonly referred to as the "racetrack effect." Griffiths and Nilson (2001, 2002; Ramsey et al. 2003) also adopted numerical methods to optimize the geometry of two-dimensional microchannel turns, and designed multi-folded channels which minimized the turn-induced spreading of a solute band in a microfluidic chip. The turn geometry was then optimized by means of a nonlinear least-squares minimization algorithm using the spatial variance of the species distribution leaving the turn as the object function. This approach yielded the turn geometry producing the minimum possible dispersion, subject only to prescribed constraints. Molho et al. (2001) employed simulation and experiment techniques to design and test a novel compensating corner geometry which reduced the racetrack effect. For situations where a constant radius turn introduces significant geometric dispersion, numerical shape optimization routines were used to determine the optimal geometries that minimize geometric dispersion while limiting reductions (the Taylor–Aris limit) in channel width. Fiechtner and Cummings (2003, 2004) used faceted design of channels for low-dispersion electrokinetic flows in
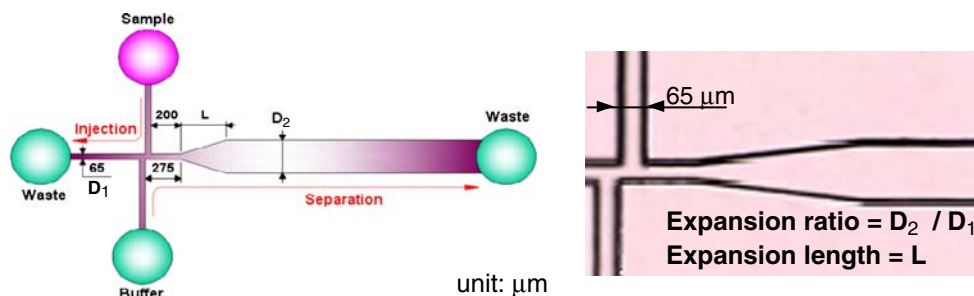
microfluidic systems. They have demonstrated the use of 2-D numerical solutions of the Laplace equation coupled with a Monte Carlo technique to model diffusion to develop a faceted design technique for minimizing dispersion. Fu et al. (2002; Tsai et al. 2005b) also considered the issue of band broadening in microfuidic systems. They performed theoretical and experimental investigations into band traverses in a folded square U-shaped channel. The authors concluded that band tilting in the detection area was corrected and the racetrack effect was reduced when the bend ratio (defined as the ratio of the microchannel width in the separation portion to the width in the turn portion) was 4:1.

In order to achieve high-resolution detection results in a chip-based microfluidic device, the sample bands injected into the separation channel must be of the correct shape and orientation. This study develops an integrated microfluidic device which combines a double-T-form injection system with an expansion chamber at the inlet of the separation channel to deliver high-quality sample plugs into the separation channel. A schematic illustration and photograph of the current microfluidic device are presented in Fig. 1. The current study develops analytical models to characterize constant expansion ratios, expansion lengths, sample plug dispersion-inducing expansion chamber, and flow fields within the expansion channel. Through simulation and experimental investigations, this study attempts to identify the optimal design and operating conditions of microfluidic capillary electrophoresis devices.

2 Experimental section

The fabrication of microfluidic chip involves standard photolithographic procedures followed by wet chemical etching as previously described (Lin et al. 2004c; Fu et al. 2005; Tai et al. 2006; Huang et al. 2006). The microchannel design, shown in Fig. 2, was transferred onto the glass substrate using a positive photoresist (AZ4620), photomask, and UV exposure. The channels are etched in a dilute BOE (6:1), stirred HF/NH$_4$F bath. Bonding of a cover plate to the glass substrate to form the closed network of channels was accomplished by fusion bonding process.

Briefly, this procedure consists of the follow steps: the two glass flats were carefully aligned, made to cling to each other using deionized (DI) water, the two glasses were held by the atmospheric pressure, and the microchip was sintered over 580°C for 10 min with a ramp rate of 5°C/min^{-1}. A sealed microfluidic device could be formed after bonding the two glass plates.

Microfluidic chip performance was monitored by a laser-induced fluorescence (LIF). The fluid sample manipulations carried out as part of the current study were observed by mercury lamp induced fluorescence using a charge-coupled device (CCD; model DXC-190, SONY, Japan) for imaging purposes. The present study used 10^{-3} M sodium borate (pH 8.5 Aldrich) as the buffer fluid, and 10^{-4} M Rhodamine B and 6.5×10^{-3} M Cy3 fluorescent dye as the sample. The sample separation exhibits four obvious peaks in the electroosmotic flow, which correspond to the three fragments of Cy3 in the hydrolysate and the single fragment of Rhodamine B within the sample. The experimental images were first captured by an optical microscope (mode E400 Nikon, Japan), then filtered spectrally (550 nm cut-on), and finally measured by a CCD device. The voltage switching apparatus was computer-controlled using programs written in-house in Labview. Finally, an APD module (Avalanche Photo-Diode, C5640-01, Hamamatsu, Japan) was used to detect the emitted optical signals. The detailed schematic representation of the experimental setup is presented in Fig. 3.
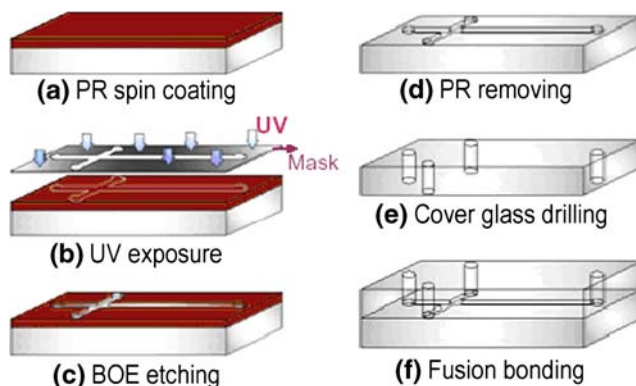

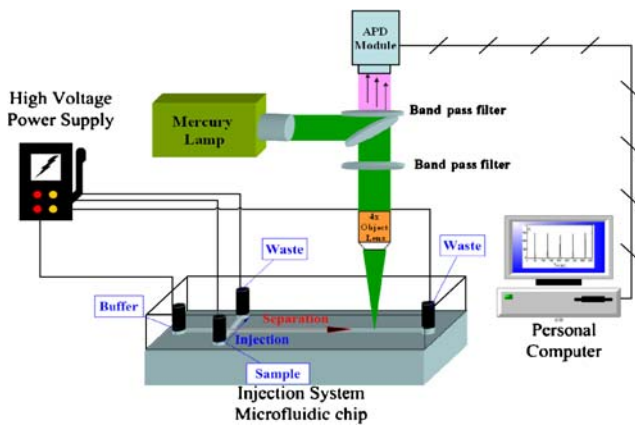Fig. 2 Overview of fabrication process for current microfluidic device

Fig. 3 Schematic illustration of current experimental setup

3 Numerical modeling

Numerical simulation of this problem requires solution of the electric potential, ζ potential, ionic concentration, velocity component, and sample concentration throughout the computational domain. A new mathematical model of the electrokinetic transport phenomena in a microfluidic dispenser is developed here with consideration of the spatial gradient of conductivity. The model considers that the processes are two-dimensional, which is very common in the modeling of similar processes. Basically, it is assumed that the variables do not exhibit significant gradients in the third direction, which is the thickness dimension. Through comparing both two- and three-dimensional models, Patankar and Hu (1998) showed this assumption to be reasonable in electroosmotic flows in similar configurations.

Since the ionic strength of the solutions employed here is relatively high, the electrical double layer (EDL) is thin. Therefore, most studies (Patankar and Hu 1998; Chein and Tsai 2004; Wang et al. 2005a,b) regarding electroosmotic flows assumed the velocity profile to be fully developed and considered the charged density to conform to Boltzmann equilibrium distribution. However, it is known that these assumptions are valid neither in turned microchannels nor in channels with irregular geometric features. Hence, these assumptions must be modified. To include those effects, current authors have previously developed physical models based on (a) the Poisson equation (ψ) for the electric potential and ζ potential for the fluid–solid boundary, (b) the Nernst–Planck equations (n^+, n^-) for the positive and negative ionic concentrations, (c) the complete Navier–Stokes equations (u, v) modified to include the effects on body force due to the electric and charge density, and (d) a sample concentration equation for the sample plug distribution. The dimensional and nondimensional equation sets applied in this study have been presented in previous studies by current authors (Lin

et al. 2002; Tsai et al. 2006a,b; Huang et al. 2006; Fu and Tsai 2007). The dimensionless form of the governing equations after dropping the head symbols can be written as:

$$\frac{\partial^2 \psi}{\partial x^2} + \frac{\partial^2 \psi}{\partial y^2} = -\frac{\kappa^2}{2}\rho_e \tag{1}$$

$$\frac{\partial n^\pm}{\partial t} + u\frac{\partial n^\pm}{\partial x} + v\frac{\partial n^\pm}{\partial y}$$
$$= \frac{1}{ScRe}\left(\frac{\partial^2 n^\pm}{\partial x^2} + \frac{\partial^2 n^\pm}{\partial y^2}\right) \pm \left[\frac{1}{ScRe}\frac{\partial}{\partial x}\left(n^\pm\frac{\partial \psi}{\partial x}\right)\right.$$
$$\left. + \frac{\partial}{\partial y}\left(n^\pm\frac{\partial \psi}{\partial y}\right)\right] \tag{2}$$

$$\frac{\partial u}{\partial x} + \frac{\partial v}{\partial y} = 0 \tag{3}$$

$$\frac{\partial u}{\partial t} + u\frac{\partial u}{\partial x} + v\frac{\partial u}{\partial y}$$
$$= -\frac{\partial p}{\partial x} + \frac{1}{Re}\left(\frac{\partial^2 u}{\partial x^2} + \frac{\partial^2 u}{\partial y^2}\right) - Gx\,\rho_e\frac{\partial \psi}{\partial x} \tag{4}$$

$$\frac{\partial v}{\partial t} + u\frac{\partial v}{\partial x} + v\frac{\partial v}{\partial y}$$
$$= -\frac{\partial p}{\partial y} + \frac{1}{Re}\left(\frac{\partial^2 v}{\partial x^2} + \frac{\partial^2 v}{\partial y^2}\right) - Gx\,\rho_e\frac{\partial \psi}{\partial y} \tag{5}$$

$$\frac{\partial C}{\partial t} + u\,\nabla C = \frac{1}{ScRe}\nabla^2 C \tag{6}$$

In the equations above, $\kappa = W \times K$, where K is the Debye–Huckel parameter given by $K = (2n_0 z^2 e^2/\varepsilon\varepsilon_0 k_b T)^{1/2}$, $1/K$ is the characteristic thickness of the charge density, $\rho_e = (n^+ - n^-)ze$ is the charge density, n^+ and n^- are the respective concentrations of the positive and negative ions, ε is the dielectric constant of the medium, ε_0 is the permittivity of a vacuum, n_0 is the bulk concentration of the ions, k_b is the Boltzmann constant, T is the absolute temperature, $L_{ref} = W$, where W is the channel height, $U_{ref} = \psi_{inlet}\varepsilon\varepsilon_0\,|\,\zeta\,|\,/\mu L$, where ψ_{inlet} is the activated potential at the inlet, Re is the Reynolds number given by $Re = \rho_f U_{ref} L_{ref}/\mu = \rho_f\left(\frac{\psi_{inlet}\varepsilon\varepsilon_0|\zeta|}{\mu L}\right)\left(\frac{L_{ref}}{\mu}\right)$, Sc is the Schmidt number given by $Sc = \mu/\rho_f D_i$, μ is the liquid viscosity, ρ_f is the fluid density, D_I is the diffusion coefficient of the sample, ζ is the surface ζ potential, p is the pressure, Gx is the ratio of the EDL energy to the mechanical kinetic energy that is given by $Gx = 2n_0 k_b T\rho_f W^2/\mu Re^2$, and finally, C is the sample concentration.

4 Results and discussion

In a microfluidic capillary electrophoresis chip, the sample injection method is one of the key elements in the sample handling process and its characteristics determine the overall quality of the separation. One of the most common sample injection methods is the cross-form injection technique. However, the high separation voltages required by this particular injection method tend to result in significant sample leakage during the separation process, which in turn reduces the detection performance of the microfluidic device (Tsai et al. 2005b). In high-resolution analysis studies, researchers have applied a double-L injection method (Fu and Lin 2003; Lin et al. 2004a,b,c; Tsai et al. 2005a, 2006a,b) in the injection and separation step to prevent sample leakage into the separation channel. Figure 4 presents the streamlines during the injection and separation steps of the double-L injection method in this proposed microfluidic device. During the injection step, the sample is loaded from channels 1 to 3 while the buffer flows in channels 2 and 4 are prevented from moving. During the separation step, the sample in the intersection is led into the separation channel (i.e. channel 4). The fluid flows predominantly from channel 2 to channel 4, while a very small flow is pushed towards the reservoirs of channels 1 and 3.

Figure 5 shows the experimental and numerical results obtained for the sample plug distribution and shape in a microfluidic device with difference expansion ratios and difference expansion lengths. For the traditional double-T injector with an expansion ratio of 1, Fig. 5(a) present that the sample plug is rather broadened and has a conical shape. When the sample plug is broadened in the detection area, the separation efficiency (or theoretical plate number) will be reduced. When the expansion chamber is inserted between the injector and the separation channel, the sample plug distribution becomes flatter and less broadened, as shown in Fig. 5(b–e). Figure 5(b) indicate that the expansion effect causes the sample plug distribution to become more convex and crooked as it travels along the expansion chamber having an expansion length of 50 μm
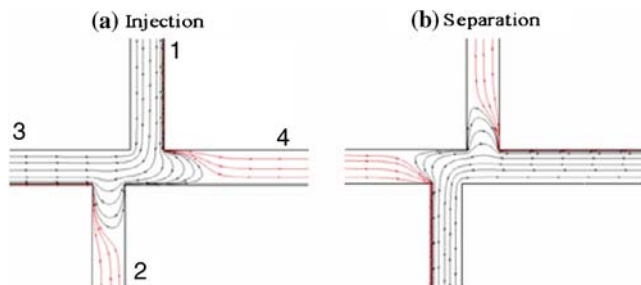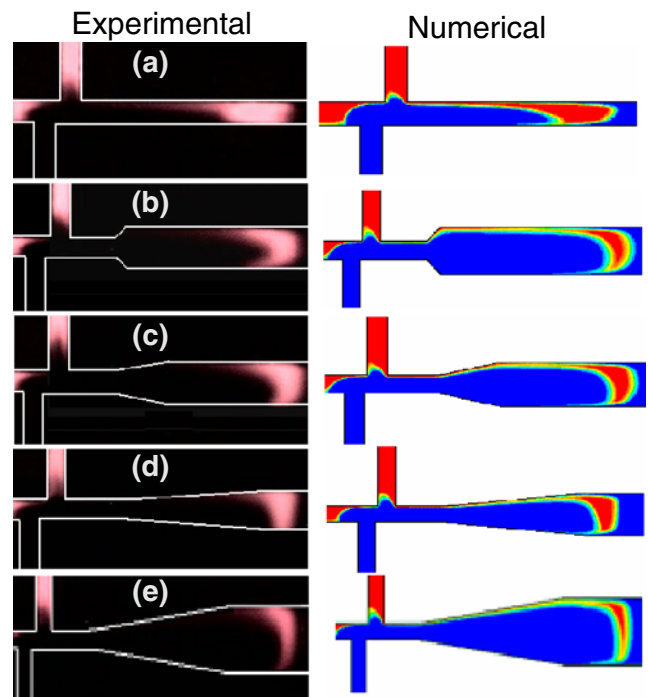

Fig. 5 Comparison of the experimental and numerical results for the sample shape in the separation processes performed in current microchips with an expansion ratio of (**a**) 1, (**b**) 2.5 with an expansion length of 50 μm, (**c**) 2.5 with an expansion length of 200 μm, (**d**) 2.5 with an expansion length of 500 μm, and (**e**) 4 with an expansion length of 500 μm

and an expansion ratio of 2.5. Figure 6(a) shows the numerical velocity profiles across the expansion chamber width at cross-sections located at the inlet (a–a), center of the expansion chamber (b–b), and outlet (c–c). Note that the chamber configuration in Fig. 6(a) corresponds to that in the Fig. 5(b), the expansion chambers have an expansion length
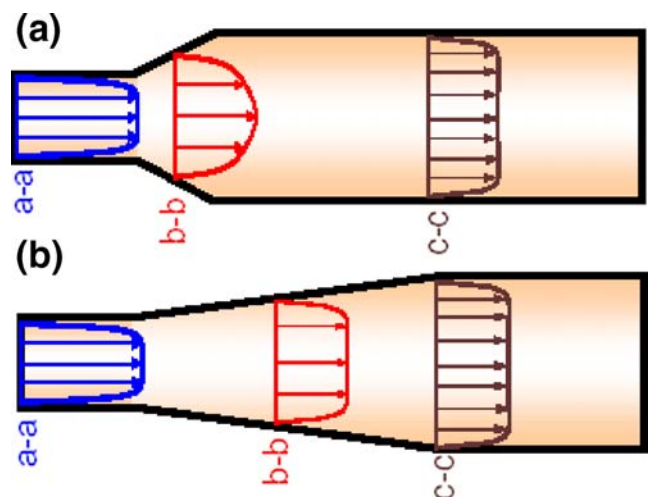

Fig. 4 Streamline plots in double-L injection method: (**a**) injection and (**b**) separation steps

Fig. 6 Comparison of velocity profiles at different cross-sections for a constant expansion ratio of 2.5 and different expansion lengths equal to (**a**) 50 μm and (**b**) 500 μm

of 50 μm and a constant expansion ratio of 2.5. In Fig. 6(a), the velocity profile is uniform and flat at the inlet region (cross-section *a–a*). As the fluid enters the expansion channel (cross-section *b–b*), the velocity profile becomes convex and gradually flattens as the fluid travels to the expansion chamber outlet. At cross-section *c–c*, it can be seen that the velocity profile is uniform and flat. The results of Fig. 6(a) suggest that an expansion chamber length of 50 μm is too short, i.e. the velocity profile has an excessive variation. The results have shown in Fig. 5(b) that a convex velocity profile can lead to a non-flat sample plug distribution. To provide a qualitative comparison of the sample plug spread, the expansion-induced variance is calculated for the sample plug passing through the expansion chamber. The normalized induced variance computed for the flow shown in Fig. 5(b) is $(\sigma/a)^2 \approx 0.12415$. Note that the detailed formulation of this variance calculation is provided in (Fu et al. 2002; Tsai et al. 2005b).

When the expansion length is increased to 200 μm at an expanding ratio of 2.5, it can be seen that the convex plug is slightly improved by the longer expansion channel (as shown in Fig. 5(c)). The normalized induced variance for the expansion chamber is found to be $(\sigma/a)^2 \approx 0.02821$. The benefit of the optimized low-dispersion expansion channel is illustrated in Fig. 5(d), which reveals that a satisfactory sample plug shape can be obtained using an expansion length of 500 μm and an expansion ratio of 2.5. The corresponding velocity profile distributions across the chamber width at difference cross-sections are shown in Fig. 6(b). The results indicate that a longer expansion length provides a sufficient distance to reduce the convex velocity profile to the flat velocity profile required to generate a suitable sample plug shape for detection purposes. A significant reduction in the convex sample
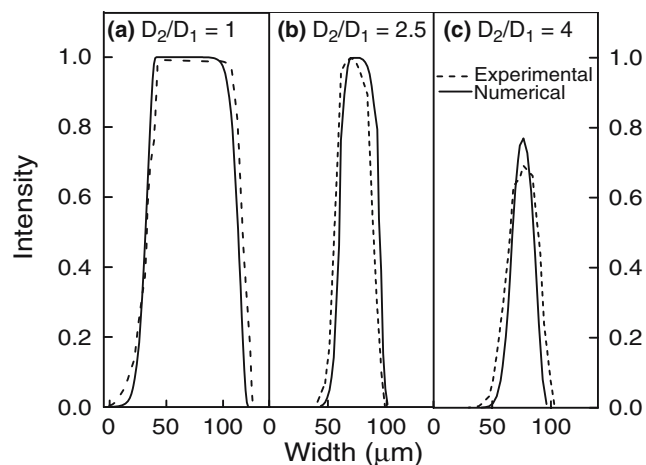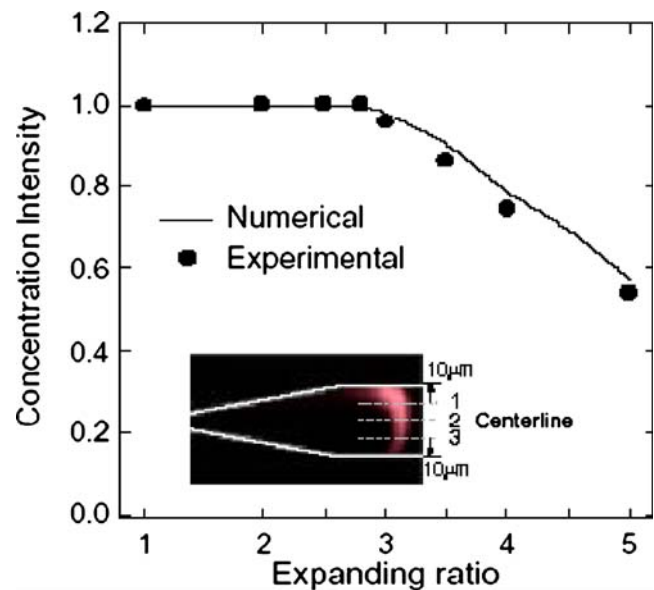

Fig. 8 Comparison of average concentration intensity of the sample plug at a position 1,000 μm downstream from the secondary T-form intersection for a constant expansion length of 500 μm and various expansion ratios

plug effect is observed and it can be seen that the sample plug which is manifested from the expansion chamber (as shown in Fig. 5(d)) is orthogonal to the walls of the separation channel. The induced variance for this particular expansion chamber configuration is only $(\sigma/a)^2 \approx 0.000502$.

Figure 7 plots the concentration intensity profiles at the centerline of the sample plug at a position 1,000 μm downstream from the secondary T-form intersection of a microfluidic device with different expansion ratios but a constant expansion length of 500 μm. It is obvious that the low expansion ratios of 1 and 2.5 still keep a high intensity sample plug in the separation channel. Note that in this figure, the experimental images obtained by mercury-lamp-induced fluorescence are given in arbitrary units and the

Fig. 7 Concentration intensity profiles at the centerline of the sample plug at a position 1,000 μm downstream from the secondary T-form intersection for a constant expansion length of 500 μm and different expansion ratios equal to (a) 1, (b) 2.5, and (c) 4
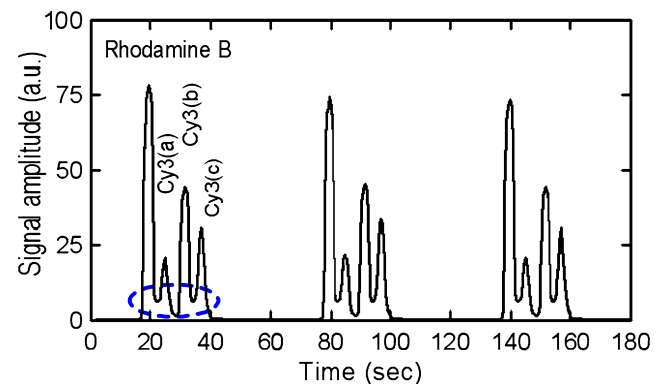

Fig. 9 Electropherogram of the separation results for Rhodamine B and Cy3 fluorescent dye samples using a traditional double-T-form separation channel (expansion ratio of 1) with an injection and separation voltage of 300 V/cm
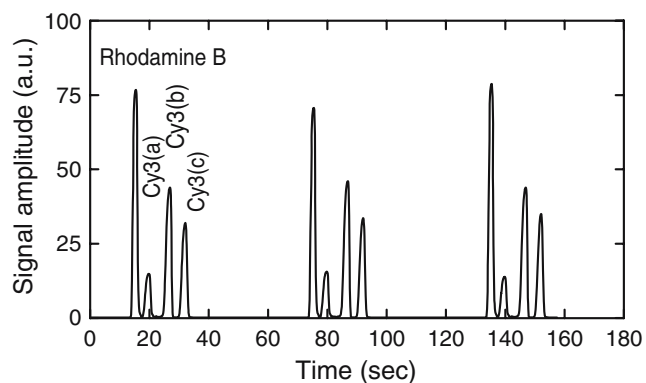
Fig. 10 Electropherogram of the separation results for Rhodamine B and Cy3 fluorescent dye samples using the proposed microfluidic device with an expansion chamber of length 500 μm and an expansion ratio of 2.5 with an injection and separation voltage of 300 V/cm

values are normalized. Meanwhile, the gray scale in the numerical simulation images represents the concentration distribution normalized relative to the initial (maximum) sample concentration. However, for an expansion ratio of 1 (i.e. no expansion effect), Fig. 7(a) indicates that the sample band distribution is rather broad. This reduces the separation efficiency and lowers the efficiency of peak intensity detection. When the expansion ratio is increased to 2.5 (as shown in Fig. 7(b)), it is clearly shown that the broad of sample plug distribution has been greatly improved. The concentration intensity remains at its highest value, but the sample plug distribution is significantly narrowed. When the expansion ratio is increased to 4 (as shown in Fig. 7(c)), the sample plug has been dispersed by a larger expansion ratio in the separation channel. The present results indicate that the concentration intensity reduces at the detection area. Hence, the detection performance of the microfluidic device is significantly degraded.

Figure 8 compares the concentration intensity of the sample plug at a position 1,000 μm downstream from the secondary T-form intersection of microchannels with different expansion ratios and a constant expansion length of 500 μm. In this figure, the concentration intensity is calculated by averaging the maximum concentration values along lines 1, 2, and 3. A small value of concentration intensity implies that the expansion chamber significantly generate excessive dispersion of the sample plug, and therefore does degrade the detection performance. As shown in Fig. 8, as the expansion ratio increases beyond 2.8, the concentration intensity steadily decreases from an initial value of one towards a value of approximately 0.55 at an expansion ratio of 5.0. From Fig. 8, it is apparent that an expansion ratio of 2.5 represents the optimal compromise for a high concentration intensity.

Figure 9 presents electropherograms generated from images collected using an APD module at the detection

area of the traditional double-T-form separation channel (expansion ratio of 1). The injection process parameters were established at 300 V/cm for an injecting time of 10 s while those of the separation process were set at 300 V/cm for 50 s. The emitted optical signals were detected at a point 3 cm away from the secondary T-form intersection of the microchannels. The sample consists of 10^{-4} M Rhodamine B and 6.5×10^{-3} M Cy3 fluorescent dye. The sample separation exhibits four obvious peaks, which correspond to the three fragments of Cy3 in the hydrolysate and the single fragment of Rhodamine B within the sample. In this figure, the peaks noted of Cy3(a) and Cy3(c) have higher baseline. The results suggest that the sample of Rhodamine B and Cy3 fragments have not completely separated at the detection area and therefore the detection result is sure to reduce the separation efficiency (or theoretical plate number).

Figure 10 presents the equivalent electropherogram when the same sample is separated with this particular expansion chamber (length 500 μm and expansion ratio 2.5) with a separation voltage of 300 V/cm. The results clearly demonstrate that the particular expansion chamber significantly confirms the superior separation and detection ability of the proposed double-T configuration microfluidic device. Therefore, this configuration is appropriate for capillary electrophoresis applications requiring a sensitive resolution of sample plug.

5 Conclusions

This paper has presented an experimental and numerical investigation about high performance sample injection and separation in microfluidic capillary electrophoresis chips. This study has developed a novel double-L injector integrating an expansion chamber at the inlet of the separation channel to improve the sample plug distribution in the separation step and increase its separation efficiency. This study has performed the experimental separation of samples consists of Rhodamine B and Cy3 fluorescent dye in order to explore the effects of the expansion chamber on the separation performance. It has been shown that an expansion chamber with an expansion ratio greater than 2.8 will induces a larger dispersive effect on the sample plug and eventually reduces the detection performance in the separation channel. A novel double-T-form injection system integrating an expansion chamber at the inlet of the separation channel with an expansion length of 500 μm and an expansion ratio of 2.5 has been developed and its performance has been analyzed. The results indicate that this microfluidic capillary electrophoresis device significantly delivers flatter sample plugs into the separation channel and hence improves the detection performance. It is the belief of current authors that the

configuration of the microfluidic capillary electrophoresis device presented in this paper provides a valuable contribution to the on-going development of the next generation of microfluidic chips.

References

J.P. Alarie, S.C. Jacobson, J.M. Ramsey, Electrophoresis **22**, 312 (2001)

S.J. Baldock, P.R. Fielden, N.J. Goddard, H.R. Kretschmer, J.E. Prest, B.J.T. Brown, J. Chromatogr. A **1024**, 181 (2004)

M.R. Bown, C.D. Meinhart, Microfluidics Nanofluidics **2**, 513 (2006)

Y.H. Chang, G.B. Lee, F.C. Huang, Y.Y. Chen, J.L. Lin, Biomed. Microdevices **8**, 353 (2006)

R. Chein, S.H. Tsai, Biomed. Microdevices **6**, 81 (2004)

J.T. Coleman, D. Sinton, Microfluidics Nanofluidics **1**, 319 (2005)

H.J. Crabtree, E.C.S. Cheong, D.A. Tilroe, C.J. Backhouse, Anal. Chem. **73**, 4079 (2001)

C.T. Culbertson, S.C. Jacobson, J.M. Ramsey, Anal. Chem. **70**, 3781 (1998)

W.B. Du, Q.H. Fang, Q.H. He, Z.L. Fang, Anal. Chem. **77**, 1330 (2005)

D. Erickson, Microfluidics Nanofluidics **12**, 310 (2005)

S.V. Ermakov, S.C. Jacobson, J.M. Ramsey, Anal. Chem. **72**, 3512 (2000)

G. Fiechtner, E. Cummings, Anal. Chem. **75**, 4747 (2003)

G. Fiechtner, E. Cummings, J. Chromatogr. A **1027**, 245 (2004)

L.M. Fu, C.H. Lin, Anal. Chem. **75**, 5790 (2003)

L.M. Fu, C.H. Lin, Electrophoresis **25**, 3652 (2004)

L.M. Fu, C.H. Tsai, Jpn. J. Appl. Phys. **46**, 420 (2007)

L.M. Fu, R.J. Yang, G.B. Lee, Electrophoresis **23**, 602 (2002)

L.M. Fu, R.J. Yang, G.B. Lee, Y.J. Pan, Electrophoresis **24**, 3026 (2003)

L.M. Fu, R.J. Yang, C.H. Lin, G.B. Lee, Y.J. Pan, Anal. Chim. Acta **507**, 163 (2004)

L.M. Fu, R.J. Yang, C.H. Lin, Y.S. Chien, Electrophoresis **26**, 1814 (2005)

Y. Gao, G. Hu, F.Y.H Lin, P.M. Sherman, D. Li, Biomed. Microdevices **7**, 301 (2005)

H. Gong, N. Ramalingam, L. Chen, J. Che, Q. Wang, Y. Wang, X. Yang, P.H.E. Yap, C.H. Neo, Microdevices **8**, 167 (2006)

S.K. Griffiths, R.H. Nilson, Anal. Chem. **73**, 272 (2001)

S. K. Griffiths, R.H. Nilson, Anal. Chem. **74**, 2960 (2002)

Y. Huang, J.M. Yang, P.J. Hopkins, S. Kassegne, M. Tirado, A.H. Forster, H. Reese, Biomed. Microdevices **5**, 217 (2003)

M.Z. Huang, R.J. Yang, C.H. Tai, C.H. Tsai, L.M. Fu, Biomed. Microdevices **8**, 309 (2006)

C.Y. Lee, C.M. Chen, G.L. Chang, C.H. Lin, L.M. Fu, Electrophoresis **27**, 5043 (2006)

F. Li, D. D. Wang, X. P. Yan, J. M. Lin, R. G. Su, Electrophoresis **26**, 2261 (2005)

J.Y. Lin, L.M. Fu, R.J. Yang, J. Micromechanics Microengineering **12**, 955 (2002)

C.H. Lin, G.B. Lee, L.M. Fu, B.H. Hwei, Microelectromechanical Syst. **13**, 923 (2004a)

C.H. Lin, R.J. Yang, C.H. Tai, C.Y. Lee, L.M. Fu, J. Micromechanics Microengineering **14**, 639 (2004b)

C.H. Lin, L.M. Fu, Y.S. Chien, Anal. Chem. **76**, 5265 (2004c)

Y. Luo, D. Wu, S. Zeng, H. Gai, Z. Long, Z. Shen, Z. Dai, J. Qin, B. Lin, Anal. Chem. **78**, 6074 (2006)

J.I. Molho, A.E. Herr, B.P. Mosier, J.G. Stantiago, T.W. Kenny, R.A. Brennen, G.B. Gordon, B. Mohammadi, Anal. Chem. **73**, 1350 (2001)

N.T. Nguyen, X. Huang, Biomed. Microdevices **8**, 133 (2006)

N.A. Patankar, H.H. Hu, Anal. Chem. **70**, 1870 (1998)

J.D. Ramsey, S.C. Jacobson, C.T. Culbertson, J.M. Ramsey, Anal. Chem. **75**, 3758 (2003)

C.L. Ren, D. Li, Anal. Chim. Acta **518**, 59 (2004)

L. Ren, D. Sinton, D. Li, J. Micromechanics Microengineering **13**, 739 (2003)

W. Saadi, S. Wang, F. Lin, N.L. Jeon, Biomed. Microdevices **8**, 109 (2006)

K. Seiler, D. Harrison, A. Manz, Anal. Chem. **65**, 1418 (1993)

D. Sinton, L. Ren, D. Li, J. Colloid Interface Sci. **266**, 448 (2003)

B.E. Slentz, N.A. Penner, F. Regnier, Anal. Chem. **74**, 4835 (2002)

C.H. Tai, R.J. Yang, M.Z. Huang, C.W. Liu, C.H. Tsai, L.M. Fu, Electrophoresis **27**, 4982 (2006)

H. Tian, C. A. Emrich, J. R. Schere, R. A. Mathies, P. S. Andersen, L. A. Larsen, M. Christiansen, Electrophoresis **26**, 1834 (2005)

C.H. Tsai, R.J. Yang, C.H. Tai, L.M. Fu, Electrophoresis **26**, 674 (2005a)

C.H. Tsai, C.H. Tai, L.M. Fu, F.B. Wu, J. Micromechanics Microengineering **15**, 377 (2005b)

C.H. Tsai, Y.N. Wang, C.F. Lin, R.J. Yang, L.M. Fu, Electrophoresis **27**, 4991 (2006a)

C.H. Tsai, M. F. Hung, L.W. Chen, C.L. Chang, L.M. Fu, J. Chromatogr. A **1121**, 120 (2006b)

C.H. Tsai, H.T Chen, Y.N Wang, C.H. Lin, L.M. Fu, Microfluidics Nanofluidics **3**, 13 (2007)

J. Wang, Z. Chen, M. Mauk, K.S. Hong, M. Li, S. Yang, H.H. Bau, Biomed. Microdevices **7**, 313 (2005a)

R. Wang, J. Lin, Z. Li, Biomed. Microdevices **7**, 131 (2005b)

K.G. Wang, S. Yue, L. Wang, A. Jin, C. Gu, P.Y. Wang, Y. Feng, Y. Wang, H. Niu, Microfluidics Nanofluidics **2**, 85 (2006)

C.W. Wei, J.Y. Cheng, T.H. Young, Biomed. Microdevices **8**, 65 (2006)

B.W. Wenclawiak, R.J. Püschl, Anal. Lett. **39**, 3 (2006)

C.H. Wu, R.J. Yang, Biomed. Microdevices **8**, 119 (2006)

Z. Wu, H. Jensen, J. Gamby, X. Bai, H.H. Girault, Lab Chip **4**, 512 (2004)

N. Xia, T.P. Hunt, B.T. Mayers, E. Alsberg, G.M. Whitesides, R.M. Westervelt, D.E. Ingber, Biomed. Microdevices **8**, 299 (2006)

Q. Xiang, B. Xu, R. Fu, D. Li, Biomed. Microdevices **7**, 273 (2005)

G.S. Zhuang, G. Li, Q.H. Jin, J.L. Zhao, M.S. Yang, Electrophoresis **27**, 5009 (2006)

H. Zou, S. Mellon, R.R.A. Syms, K.E. Tanner, Biomed. Microdevices **8**, 353 (2006)